Sensitivity of the pseudo-global warming method under flood conditions: A case study from the Northeastern U.S.

Zeyu Xue[1] and Paul Ullrich[1]

[1]Atmospheric Science Graduate Group, University of California, Davis, Davis, California

Correspondence: Zeyu Xue (zyxue@ucdavis.edu)

Abstract. Intensified extreme precipitation and resulting flooding are among the most impactful consequences of climate change, especially over the northeastern US (NEUS). To project and understand the impacts of climate change (or related climate perturbations) on extreme weather events as they may occur in the future, the Pseudo-Global Warming (PGW) method has been employed with great success. However, it has never been ascertained to what degree the conclusions from PGW
5   studies are sensitive to the design of the PGW experiment. Consequently, three key questions related to the application of the PGW method remain unanswered: At what spatial scale should climate perturbations be applied? Among the different meteorological variables available, which should be perturbed? And will PGW projections vary significantly under different experiment designs? To begin to address these questions, we examine the sensitivity and robustness of conclusions drawn from the PGW method over NEUS by conducting multiple PGW experiments. The results show that the projections of precipitation
10 and other essential variables are consistent at the regional mean scale, with a relative difference of much less than 10%; however, different experimental designs nonetheless cause significant displacements among storm events. Several previously assumed advantages of modifying temperature at the regional mean scale do not appear to hold, such as the preservation of geostrophic balance. Also, we find the regional mean perturbation produces a positive precipitation bias due to overestimated warming over the ocean. Overall, PGW experiments with perturbations from temperature or the combination of temperature
15 and wind at the gridpoint scale are both recommended, depending on the research target. The first approach can isolate the spatially-dependent thermodynamic impact, and the latter incorporates both the thermodynamic and dynamic impacts.

1 Introduction

Historical observations and model projections highlight the significant risk that climate change poses for society (Pachauri et al., 2014). Among the many consequences of climate change, the intensification of extreme precipitation is considered to be
20 one of the most impact-relevant (Pfahl et al., 2017). Within the United States, confidence is highest that the northeastern U.S. (NEUS) will experience the most significant intensification of extreme precipitation, with observations alone indicating that the most intense daily precipitation events in this region (those above the 99th percentile of daily precipitation) increased by more than 70% from 1958 to 2012 (Melillo et al., 2014). Accordingly, severe flood risk is also increasing, carrying with it increased risk of loss of life and infrastructural damage or failure (Hirabayashi et al., 2013; Frumhoff et al., 2007; Narayan et al., 2017).
25 The NEUS is at especially high risk, considering it is the most populated and developed region in the U.S. (Hobbs, 2008;

US Bureau of Economic Analysis, 2016). Therefore, robust and reliable projections of extreme precipitation and associated flooding are urgently needed in this region for adaptation planning.

Climate models are the most widely used tool for projecting climate change and its impacts (Kharin et al., 2007; Wagener et al., 2010; Frumhoff et al., 2007). And although significant progress has been made in improving models' physical consis-
30 tency, persistent issues include large uncertainties and insufficient model resolution for representing extremes and regional impacts (Xu and Yang, 2012; Deser et al., 2020; Dai et al., 2020). These uncertainties mainly consist of scenario uncertainty, model uncertainty, and internal variability (Xie et al., 2015; Hawkins and Sutton, 2009; Deser et al., 2012). Among these, internal variability is generally deemed as the most significant source of uncertainty in the near-term and accounts for approx-imately half of the inter-model spread across North American precipitation projections in the next fifty years (Deser et al.,
35 2020, 2014).

Climate model experiments with the Pseudo-Global Warming (PGW) method enable targeted exploration of regional impacts from future climate change, while avoiding the large ensembles typically required to address internal variability (Schär et al., 1996; Xue and Ullrich, 2021b). Unlike traditional dynamical downscaling, which drives regional climate models (RCMs) using the outputs from global climate models (GCMs) to produce regional climate projections, the PGW method employs initial and
40 boundary conditions from reanalysis data, perturbed using estimates of changes from GCMs. It ensures that simulated features essentially follow the similar track as historical events – and can directly address questions about how climate change would affect a given feature if the same large-scale patterns were to return in the future. The PGW framework allows for significant flexibility with respect to the choice of spatial scale and choice of modified variables. Initially, the PGW method was employed to examine how do atmospheric moisture and precipitation response to a regional uniform temperature increase (Schär et al.,
45 1996; Frei et al., 1998). In these first PGW studies, only a uniform temperature perturbation was added because it represented the leading order behavior from climate change. Later studies extended this approach using a temperature perturbation that depended on both time and pressure (Hill and Lackmann, 2011; Yates et al., 2014; Mallard et al., 2013b, a; Ullrich et al., 2018; Xue and Ullrich, 2021b). By using a perturbation that was constant along pressure surfaces, it was anticipated that potential loss of geostrophic balance in the boundary conditions from inconsistency in the dynamical and thermodynamical fields could
50 be avoided (Schär et al., 1996; Frei et al., 1998; Blumen, 1972). Additionally, a regionally-homogeneous perturbation applied only to the temperature field was assumed not to impact the dynamical fields, since geostrophic wind speeds are determined by the unmodified geopotential gradients. This approach was designed to avoid the well-documented uncertainties that persist in future projections of dynamical fields (Vecchi and Soden, 2007; Garner et al., 2009). Nonetheless, others have performed PGW simulations that modify both the thermodynamic and dynamic variables at each gridpoint to better reflect the dynamical
55 influence of climate change (Kimura et al., 2007; Kawase et al., 2009; Denamiel et al., 2020). Altering the dynamic fields (i.e., the wind speed and direction) has the potential to displace extreme weather events and so provide insights into how climate change would alter the tracks of these features. However, concerns have persisted that this approach does upset geostrophic balance, and introduces inconsistencies between the dynamic and thermodynamic fields which could generate spurious gravity waves from the boundary of the simulated domain. While these waves are filtered to some degree by numerical and physical

60 viscosity in the regional climate model, care should be taken to ensure that this unphysical noise does not contaminate the simulation.

The most significant advantage of the PGW method is that it captures the large scale circulation of events that have been observed historically, and so avoids the uncertainty that a particular event is a product of model biases in the GCM. These biases in the large-scale circulation forcing provided by GCMs are generally deemed to be one of the most significant sources

65 of biases in dynamical downscaling (Wang et al., 2004; Sato et al., 2007). Furthermore, because PGW simulations are driven by historical reanalysis data plus the meteorological perturbations caused by climate change, they can directly answer the crucial question "what will historical extreme weather events look like under climate change?" This has led to growing popularity of the PGW method, since hazard management such as flood control often uses "model events" that are based on infamous historical disasters (Burns et al., 2007; Milly et al., 2008). The PGW method has a number of additional advantages, such as only

70 requiring monthly mean GCM projections to provide climate perturbations, making it much easier to employ in conjunction with large ensemble or multi-model GCMs.

Although the PGW method has grown in popularity in the past decade, there is still little guidance on best practices for the use of the PGW method. As noted already, the PGW method offers substantial flexibility in how it is employed: there is freedom to choose which boundary conditions to modify, whether or not the perturbations have space and time dependence, and how other

75 inputs such as land use, greenhouse gas concentrations, or aerosols are modified. While these choices have led to substantial divergence in experimental design throughout the PGW literature, it is entirely possible that different choices may produce different conclusions. Altogether, these observations suggest the need for a sensitivity analysis of different PGW methods to examine the uncertainties and robustness of PGW simulations, and to subsequently provide guidance on PGW experimental design. Of course, a single study is insufficient to comprehensively evaluate the sensitivity when employing PGW over multiple

80 regions of different climatological character that considers domain size, choice of reanalysis data, modified variables, temporal and spatial dependence of the climatological perturbations, regional model tuning parameters, and other such options. In this paper we thus consider a far narrower scope, and focus our investigation on a single case study, with the expectation that this work could frame future investigations on this topic.

Given that storms and subsequent flooding are the most popular events in the PGW literature, and are known to be sensitive

85 to both thermodynamic and dynamic changes (Frei et al., 1998; Kawase et al., 2009; Knutson et al., 2013; Mallard et al., 2013b; Yates et al., 2014), they provide a suitable context for investigating sensitivities in the PGW method. In this paper we perform an ensemble of PGW simulations that involve three major flood events over NEUS, each the product of different meteorological drivers, including the October 2005 flood (October 7th to 17th), the New England flood of May 2006 (May 12th to May 20th) and the 2006 Mid-Atlantic United States flood (June 23rd to July 5th). Our simulation ensemble varies the modified

90 variables (temperature, wind, geopotential height, and sea surface pressure) and the method in which the modification is applied (perturbation is calculated at the regional mean or each gridpoint). Our focus in the comparison is primarily on those simulations where temperature is modified at either regional mean or at each gridpoint, and those simulations conducted with perturbations to different meteorological variables at each gridpoint. This paper aims to answer following major questions: First, are PGW

simulations sensitive to the spatial scale of climate perturbations? Second, besides temperature, which meteorological variables
95 should be modified in PGW experiments? And finally, what is the recommended guidance for the design of PGW simulations?

2   Data and methods

2.1   Experiments design

Our simulations use the Weather Research and Forecasting (WRF) model 3.9 (Skamarock et al., 2008; Powers et al., 2017)
with hybrid mass-based coordinate to simulate the 16-month period between April 2005 and July 2006. This period is chosen
100 as it includes the three major flood events in Table 1. Historical and future simulations are driven by reanalysis data without
and with perturbations to meteorological variables obtained from GCMs. WRF has been used extensively for regional climate
modeling, in each case demonstrating reasonable fidelity in reproducing regional climatology (Knutson et al., 2013; Heikkilä
et al., 2011; Rasmussen et al., 2011; Dai et al., 2020). Our simulations use the parameterization set employed in our previous
PGW studies (Ullrich et al., 2018; Xue and Ullrich, 2021b), as this choice has been demonstrated to be both robust and
105 produce good performance over the NEUS. Additionally, all simulations use the Community Land Model. An investigation of
the sensitivity of the PGW simulations to parameterization set and land model is beyond the scope of the present study, as we
expect this choice to be orthogonal to our conclusions.

All PGW experiments cover two periods: the historical flood period (2005 April to 2006 July) and the mid-21st century
"returned" flood period (2055 April to 2056 July). Following (Jerez et al., 2020), the first six months of the simulation serve as
110 the spin-up period, so as to ensure the meteorology and land model are consistent. Two nested domains are employed that cover
the NEUS, with resolutions of 30 and 10 km respectively, as shown in Figure 1. In this study, without notation, our analysis is
based on the inner domain, which covers most of the NEUS at the finer resolution. Our analysis of dynamic perturbations (wind
and sea level pressure) will be over the whole domain because of their connection with the broader atmospheric circulation. In
WRF, spectral nudging is employed at its default relaxation level. 30-arc second resolution United States Geological Survey-
115 based geography data provides geographic data such as land use, elevation, green fraction, and leaf area index data.

2.2   Methodology and modified forcings

The 6-hourly ECMWF Reanalysis 5th Generation (ERA5) reanalysis is employed to provide initial and boundary conditions.
ERA5 is a next-generation reanalysis product that replaces the ERA-Interim reanalysis (European Centre for Medium-Range
Weather Forecasts, 2020b; Hersbach et al., 2020), incorporating improved data assimilation, core dynamics, model physics,
120 temporal and spatial resolution. ERA5 has shown to represent low-frequency variability well, and so is expected to capture
historical meteorological conditions with high fidelity (Hersbach et al., 2020; Tarek et al., 2020; Dullaart et al., 2020).

For our future PGW simulations, the initial and boundary conditions are adjusted by adding monthly mean and ensemble
mean climate perturbations from the Community Earth System Model (CESM1) Large Ensemble (LE) dataset (European
Centre for Medium-Range Weather Forecasts, 2020a) under Representative Concentration Pathway (RCP) 8.5. The climate

Table 1. The three flood periods studied in this paper.

Flood Periods	Duration	Meteorological Cause	Region
Northeast U.S. flooding of October 2005 (2005 Oct Flood)	October 7th to 17th, 2005	A larger extratropical storm in the eastern Gulf of Mexico absorbed a part of Tropical Storm Tammy and connected with a cold front system over the Mid Atlantic region then a low pressure center staying over the Long Island dragged a huge amount of moisture from the western Caribbean Sea and brought heavy rainfall to the NEUS (Stewart, 2006; Beven, 2006; Oravec, 2006; Station, 2005; Stuart and Grumm, 2009).	The interior New England, as well as over parts of New Jersey and New York.
New England Flood of May 2006 (2006 May Flood)	May 12th to May 20th, 2006	An unusually strong low pressure system that stalled over the central United States pull huge amounts of moisture from the Atlantic Ocean to the NEUS (Center, 2006c, d; Stuart and Grumm, 2009; Agel et al., 2015).	The New England, especially in New Hampshire and Massachusetts.
2006 Mid-Atlantic United States flood (2006 June Flood)	June 23rd to July 5th, 2006	The tropical low over the North Carolina coast brought constant tropical moisture to the Mid-Atlantic region which is blocked by the stalling of the jet stream over the west of Appalachian Mountains and the Bermuda High over the Atlantic Ocean thus formed huge amounts of rainfall (Center, 2006a, b; Stuart and Grumm, 2009).	The Mid-Atlantic region.
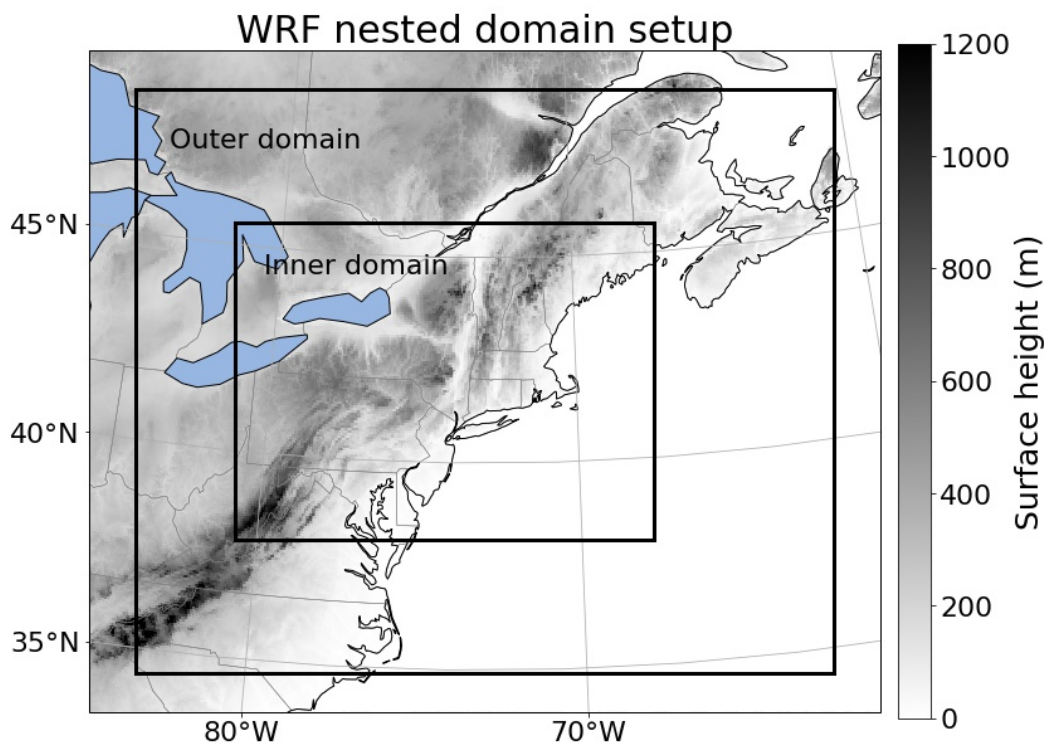
Figure 1. The WRF domain for all simulations in this study. Shading indicates the surface elevation. Grid spacing in the outer (inner) domain is 30 km (10 km).

125   perturbations are calculated by taking the difference between meteorological fields from 2030-2059 and 1980-2009. These long periods are used to reduce noise from internal variability. In all cases, perturbations are computed as a function of month (i.e., each of January, February, etc. has its own climatological perturbation), and linearly interpolated in time. CESM1 is employed here since it is a high-quality model with demonstrable performance over the NEUS (Kay et al., 2015; Swann et al., 2016; Sillmann et al., 2013; Karmalkar et al., 2019; Xue and Ullrich, 2021a). Further, its initial condition ensemble contains

130   forty instances, allowing us to mitigate noise from internal variability, and providing all necessary meteorological variables for this study. Moreover, since the parameterization set and land model in our WRF simulations are also used in CESM, we can maintain some degree of consistency between the forcing data and the regional climate simulation.

2.3   Ensemble design

Following (Schär et al., 1996) and the numerous PGW studies since (Kawase et al., 2009; Knutson et al., 2013; Mallard et al.,

135   2013b; Yates et al., 2014; Xue and Ullrich, 2021b; Ullrich et al., 2018), we conduct and compare five PGW experiments that vary the modified meteorological fields at the gridpoint level, and one additional experiment that applies the thermodynamic modification at the regional mean scale. All experiments investigated are described in Table 2. 3D variables modified in these

Table 2. Ensemble Design

Simulation	Modified variables	Perturbation scale
PGW_T_ regional	Air temperature at each pressure level	Regional mean
	Sea surface temperature	
PGW_T_gp	Air temperature at each pressure level	Gridpoint
	Sea surface temperature	
PGW_T_WIND_gp	Air temperature at each pressure level	Gridpoint
	Wind at each pressure level	
	Sea surface temperature	
PGW_T_ZG_gp	Air temperature at each pressure level	Gridpoint
	Geopotential height at each pressure level	
	Sea surface temperature	
PGW_T_SLP_gp	Air temperature at each pressure level	Gridpoint
	Sea level pressure	
	Sea surface temperature	
PGW_T_WIND_ZG_SLP_gp	Air temperature at each pressure level	Gridpoint
	Wind at each pressure level	
	Sea level pressure	
	Sea surface temperature	

experiments are air temperature (T), zonal and meridional wind (UA and VA), and geopotential height (ZG). 2D variables modified in these experiments are sea-level pressure (SLP) and sea surface temperature (SST). In all PGW simulations relative humidity is assumed constant, meaning specific humidity is updated as a function of the modified temperature. Constant relative humidity is a common assumption under PGW since it is largely unaffected by climate change in moist regions, particularly in the lower troposphere. Greenhouse gas concentrations are also updated in WRF, in accordance with those prescribed by the RCP8.5 emission scenario.

3 Result

3.1 Model validation

Before examining the sensitivity of different PGW simulations to experimental design, we first validate the ability of our historical WRF simulation to simulate the observed surface temperature and precipitation during the events of interest. WRF is the most widely-used regional climate model in the PGW literature and has consistently demonstrated good performance for simulating regional climate, with appropriate parameterizations (Kharin et al., 2007; Denamiel et al., 2020; Lackmann, 2015), and so we keep our validation brief. For comparison, we use the Climate Prediction Center unified gauge-based analysis precip-
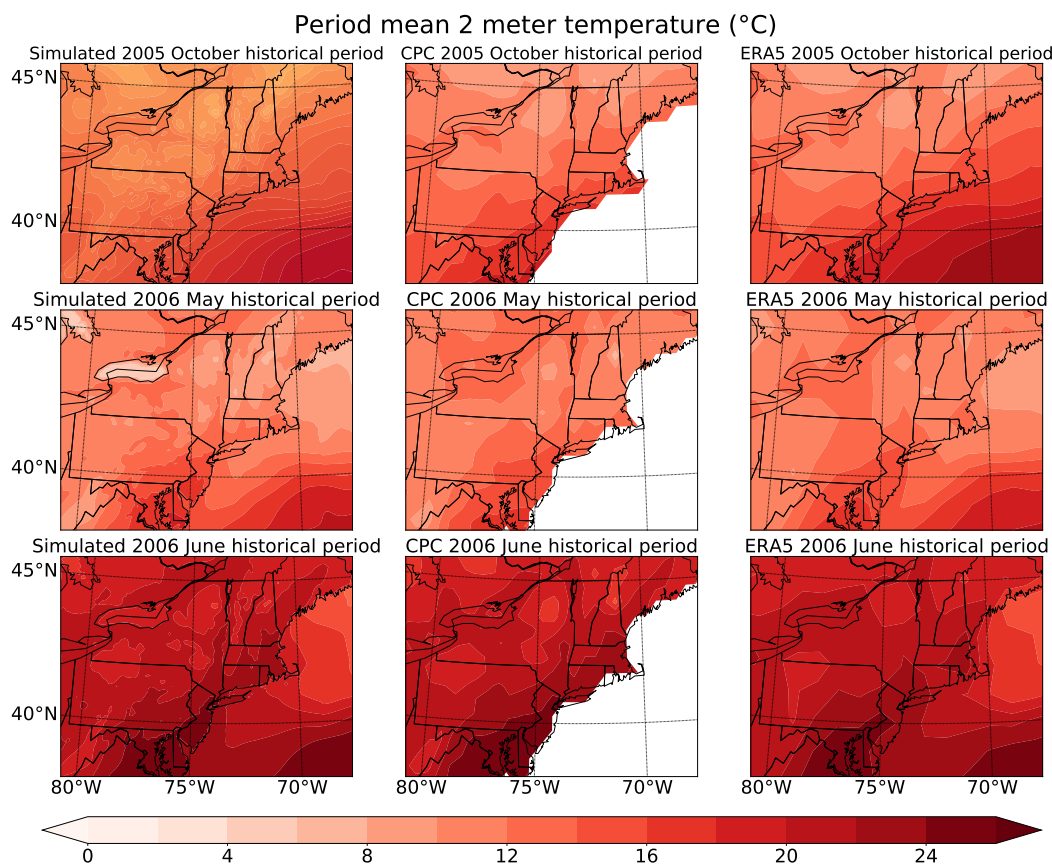
Figure 2. Average 2-meter temperature (°C) over the inner domain from our historical PGW simulation, CPC Global Temperature data and ERA5 reanalysis data during flood periods.

itation data (CPC) (NOAA Physical Sciences Laboratory, 2020), the Integrated Multi-satellite Retrievals for GPM (IMERG) (Huffman et al., 2015; The National Aeronautics and Space Administration, 2021), and the driving reanalysis (ERA5) (European Centre for Medium-Range Weather Forecasts, 2020b). Fig. 2 shows that the simulated temperature at 2 meter is similar to its driver (ERA5). In Fig. 3, it's clear that WRF's simulated precipitation is similar in magnitude and structure to the CPC and

155   IMERG data, and exhibits finer structure than the ERA5 precipitation. The finer grid spacing of the WRF simulation further enables us to better capture the locations of high precipitation intensity, particularly near the coasts. Based on this comparison, it's clear that both the surface temperature and precipitation match well with observations during the three flood periods.

3.2 PGW simulations with regional mean vs. gridpoint temperature perturbations

Given the direct impact on near-surface temperatures and indirect impact on precipitable water content, modifying temperature

160   is expected to have the most significant effect in these PGW experiments. As mentioned earlier, while some past studies apply
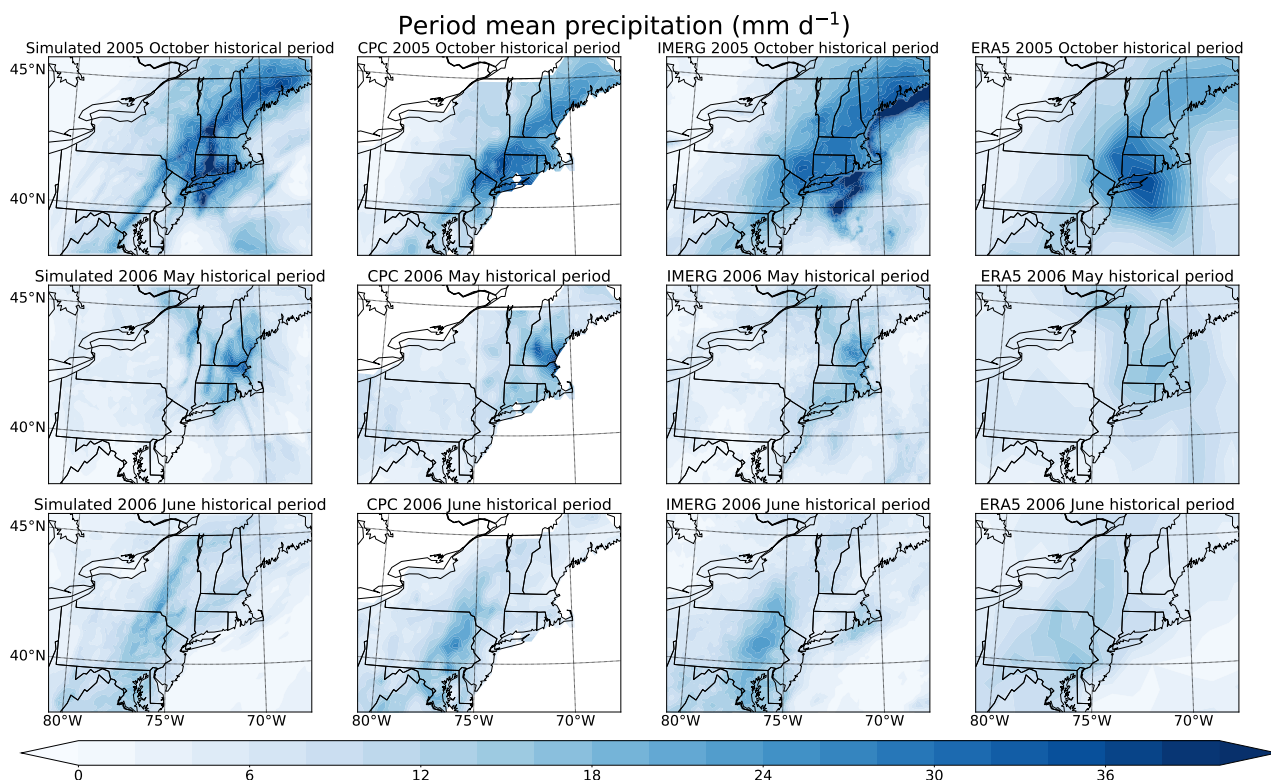
Figure 3. Average precipitation (mm d^{-1}) over the inner domain from our historical PGW simulation, CPC observational data, IMERG and ERA5 reanalysis data from during flood periods.

a regional mean perturbation to temperature (1D space + 1D time), others apply these perturbations at every grid point (3D space + 1D time). In this section, we investigate the difference between these two methods.

Figure 4 shows the flood period mean temperatures from the simulation with regional mean perturbations and the temperature delta from the simulation with gridpoint perturbations. As expected, the regional mean simulation exhibits more uniform
165   temperature differences, especially when looking over the whole simulation period (Fig. S1). However, this outcome is somewhat inconsistent with GCM projections, which generally indicate enhanced warming over land and suppressed warming over the ocean as a consequence of differences in heat capacity and the redistribution of temperature during storm events. Precipitation amounts are subsequently affected by this difference: As the ocean is the primary source of moisture of storm events (Fig. S2), and most precipitation occurs over the coast (Fig. 5), the simulation with regional mean temperature perturbations pro-
170   duces more precipitation in the future than the gridpoint perturbation experiment (regional period mean precipitation increase from 12.69 mm d^{-1}, 7.19 mm d^{-1}, and 7.83 mm d^{-1} to 13.86 mm d^{-1}, 7.43 mm d^{-1}, and 7.88 mm d^{-1} in each flood period, as in Fig. 6). Notably, the first flood event (October 2055) exhibits a greater difference between regional and gridpoint perturbation experiments (9.22 %) compared with the other two events (3.38 % and 0.61 %). Nonetheless, the relative displacement of the

storm pattern is more apparent than the regional mean precipitation differences. The greater impact of experimental design on

175 the first storm event appears to be a result of two factors: first, the strong frontal system associated with this event is associated with more intense uplift (Fig. S10); and second, the strong on-shore flow (Fig. S9) associated with this event greatly amplifies the on-shore water vapor transport by the storm. The vertical pressure velocity is not significantly modified in each PGW simulation, suggesting that this increase in precipitation is primarily thermodynamic (Norris et al., 2019).

If we look at the entire simulated period, the PGW_T_regional simulation has a far larger regional mean precipitation

180 increase compared with PGW_T_gp over the sea (with 12.12% relative change) than over the land (with 2.49% relative change). This result is because the regional mean simulation leads to more warming over the ocean than the land, and so with relative humidity held constant, there is more precipitable water and vapor transport in the regional mean simulation over the ocean, but less over the land (Fig. S2). This observation also explains why the third flood event has the smallest precipitation increase, since it features more inland precipitation than the other two (Fig. 5). The period maximum regional mean precipitation also

185 reflects these observations (Fig. 6).

3.3 Gravity wave noise

As mentioned earlier, one concern with the use of gridpoint level perturbations is the possible generation of gravity wave noise due to geostrophic adjustment. However, high-frequency wave-like noise (i.e., transient inertia-gravity waves) are apparent in the meteorological field examined (sea level pressure) (Xue and Ullrich, 2022) in both PGW_T_regional and PGW_T_gp at

190 approximately the same magnitude, if fields are examined on hourly scales. This conflicts with the assumption in previous studies that regionally-uniform or latitudinally-uniform temperature perturbations inherently avoid geostrophic imbalance and resulting adjustments (Schär et al., 1996; Frei et al., 1998; Hill and Lackmann, 2011; Yates et al., 2014; Mallard et al., 2013b; Ullrich et al., 2018). However, none of PGW studies cited identify that a uniform temperature perturbation can induce such meteorological noise. This is likely an oversight, since this noise is not apparent at the period mean scale (Fig. S3). Indeed, it

195 appears that the wave-like noise is attributed to and magnified by the development of storm events within the inner domain, when significant advection of energy and momentum is present. In WRF, boundary conditions are specified and nudged based on the input forcing (here the historical reanalysis data with climate perturbations) only within the outer-most domain (Skamarock et al., 2008); however, within the inner domain, except for the most peripheral grid points, meteorological fields are much less constrained by the boundary conditions provided and can significantly depart from the forcing data (Skamarock

200 et al., 2008). Inconsistencies among meteorological fields then provide a possible reason for why the wave-like noise still persists in PGW_T_regional, even though geostrophic balance holds in the initial and boundary conditions. Furthermore, the observed noise is enhanced by strong advection during these extreme weather events, as it is much more obvious during these storm events (Xue and Ullrich, 2022). Moreover, while it is normally assumed that dynamical fields are unchanged under a uniform temperature perturbation (Schär et al., 1996; Frei et al., 1998; Hill and Lackmann, 2011; Yates et al., 2014; Mallard

205 et al., 2013b; Ullrich et al., 2018), we notice that both the wind and sea level pressure of PGW_T_regional vary from the historical run (Fig. S11 to S13) and their differences are even comparable to PGW_T_gp's because of the redistribution of energy and momentum during the weather events. For example, the temperature advection over the ocean during the storm will

bring more energy to the coast region and so can intensify local convection processes, reduce the sea level pressure and alter the wind fields. Since PGW_T_regional may overestimate precipitation, and does not solve the problem of gravity wave noise, we do not recommend this experimental configuration.

3.4 Sensitivity of PGW simulations to choice of perturbed meteorological fields

We now turn our attention to comparing simulation response when different sets of climatological fields are modified at the gridpoint level. In this case, the baseline simulation only applies temperature perturbations at each gridpoint and the effect from modifying other meteorological fields is then ascertained by comparing with the baseline. As we can see in Fig. 6, perturbations to the meteorological fields used do produce a spread in regional precipitation rates and totals; however, at the regional mean scale, this spread is fairly small across simulations, with different choices producing precipitation differences within 10% of the baseline. However, we do observe that the October flood event is more sensitive to the experimental setup than the other two events. The reasons for this difference will be discussed in the following sections.

3.4.1 Sensitivity of PGW simulations to inclusion of wind perturbations

When wind perturbations are included, all PGW simulations generally simulate more precipitation over land, especially along the coast of the inner domain. The coastal region also experiences the most rainfall in each historical period (Fig. 6 and 8) because precipitation in this region is largely driven by the transport of precipitable water from the ocean to land (Fig. S2). As the land and sea areas are found in the northwestern and southeastern portions of our domain, respectively, both positive meridional wind and negative zonal wind perturbations over the sea increase advection of precipitable moisture into the coastal region of the inner domain, in turn enhancing precipitation. For example, during the 2055 October flood period, the zonal wind is modified with a strong negative perturbation (with a regional mean of -0.15 m s^{-1}), much larger than the positive meridional wind perturbation (0.014 m s^{-1}), corresponding to enhanced onshore flow. This leads to more vapor advection and enhanced precipitation over the coastal region of the inner domain, with a 0.71 mm d^{-1} regional mean land precipitation increase (Fig. 6). Additionally, during this event, the addition of the wind perturbation reduces precipitation over the sea, as it carries moisture onto land. During the other two flood periods, both the meridional and zonal wind perturbations are much smaller than 0.1 m s^{-1}, so the subsequent overland precipitation increase is also much smaller (a regional mean increase of 0.16 and 0.19 mm d^{-1}). The magnitude of these wind perturbations explains why, under this experiment, the first flood event shows a stronger future response. Considering the whole simulation period, there are slightly positive meridional wind perturbations (with a regional mean of 0.054 m s^{-1} and 0.016 m s^{-1} over the sea and land) and negative zonal wind perturbations (with regional mean of -0.039 m s^{-1} and -0.023 m s^{-1} over the sea and land), which results in a slight precipitation increase (with regional mean of 0.13 mm d^{-1} over both the sea and land). Since the wind perturbation conveys useful information pertaining to climate change's impact on atmospheric dynamics, we acknowledge it is useful to include in general PGW studies. However, as mentioned earlier, significant uncertainties persist regarding future dynamical change, and so care should be taken when it is included.
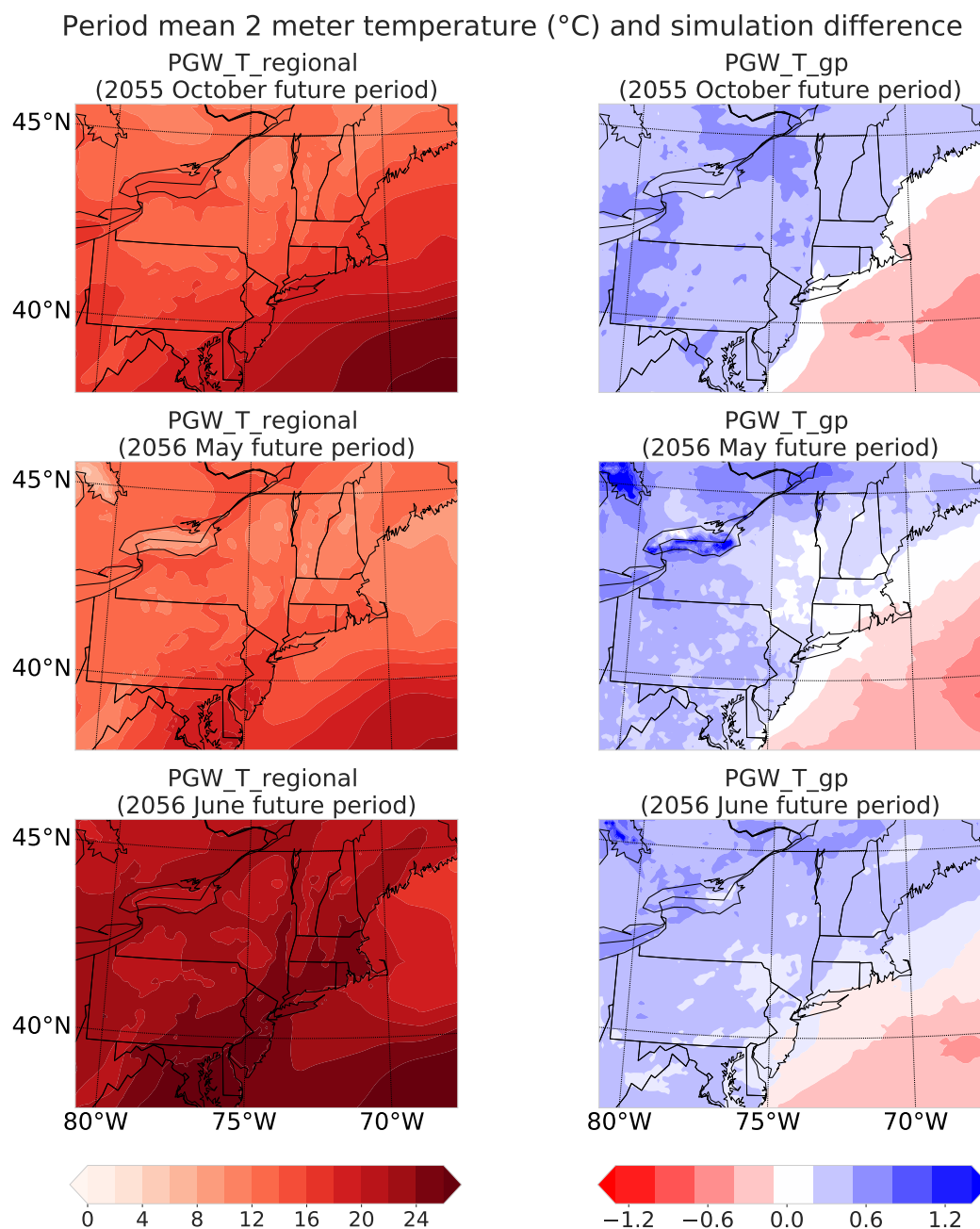
Figure 4. (Left) Period mean 2 meter temperature (°C) over the inner domain from the simulation with temperature perturbation at regional mean scale. (Right) Difference between the period mean 2 meter temperature (°C) from the gridpoint perturbation simulation and regional mean simulation from the left column.
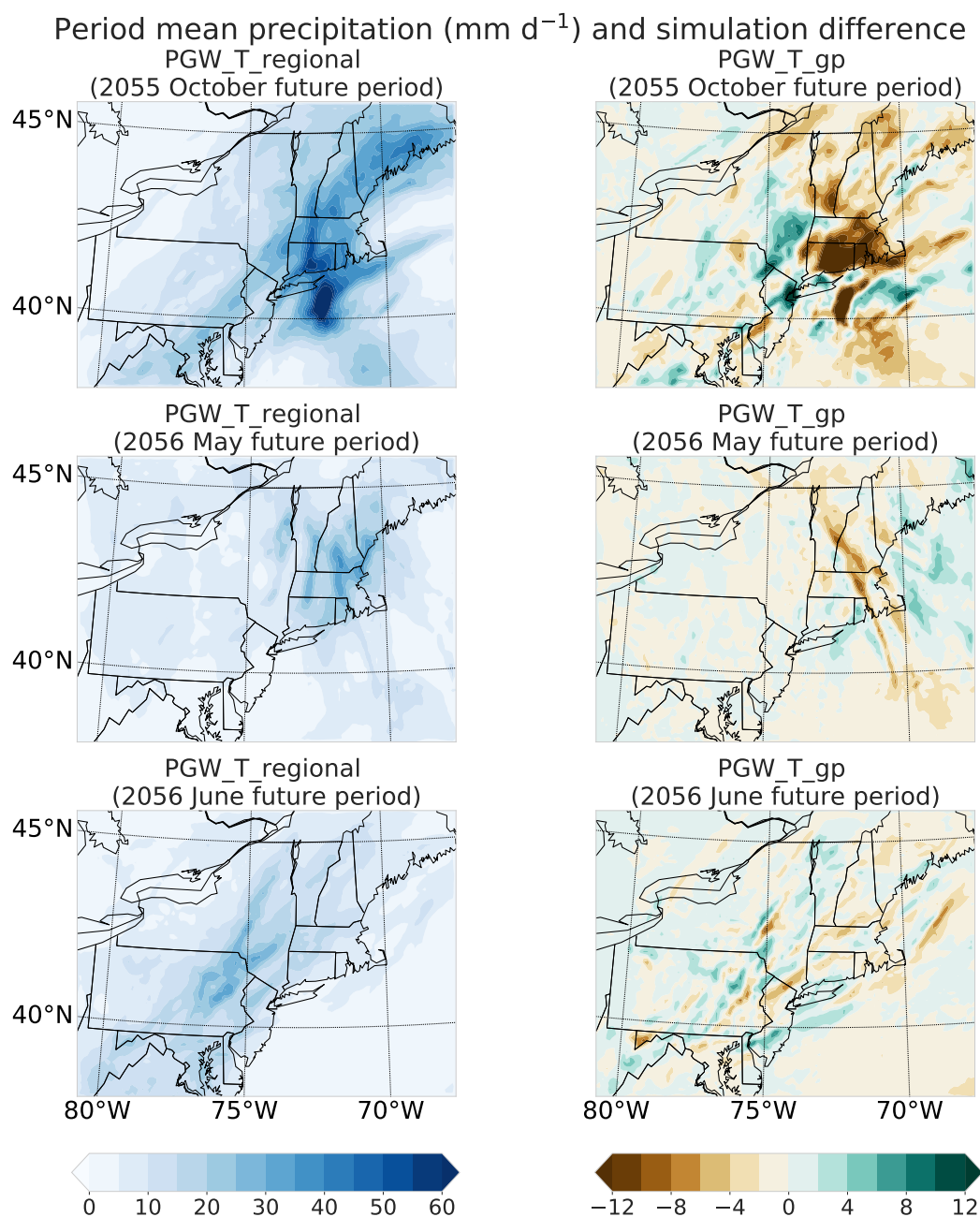
Figure 5. Period mean precipitation (mm d^{-1}) over the inner domain from the simulation with temperature perturbation at regional mean scale, and simulated perturbations in the simulation with temperature perturbation at each gridpoint.
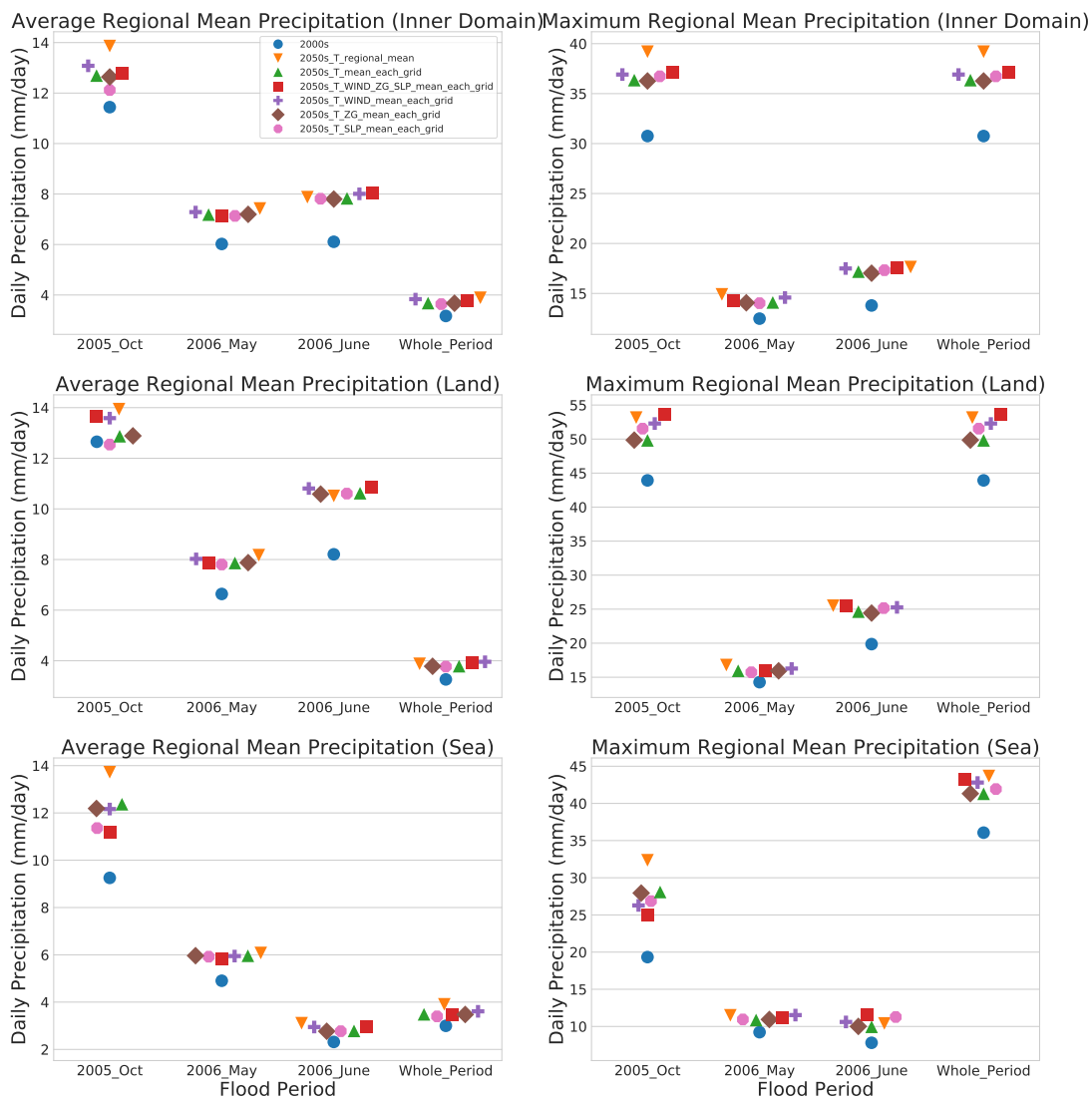
Figure 6. Period regional mean precipitation (mm d^{-1}) over the inner domain, its land area and sea area from the all PGW simulations with different perturbation modification methods.
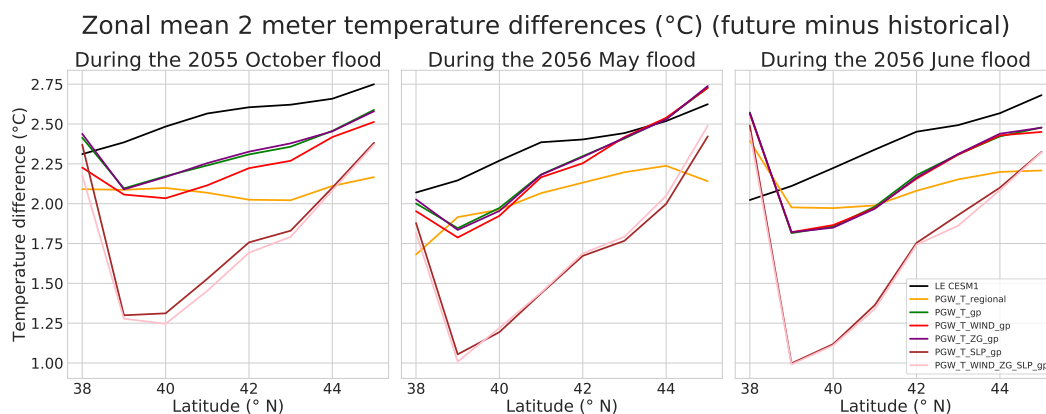
Figure 7. Period zonal mean temperature at 2 meter differences (°C) over the inner domain. The difference is with respect to the historical flood period.
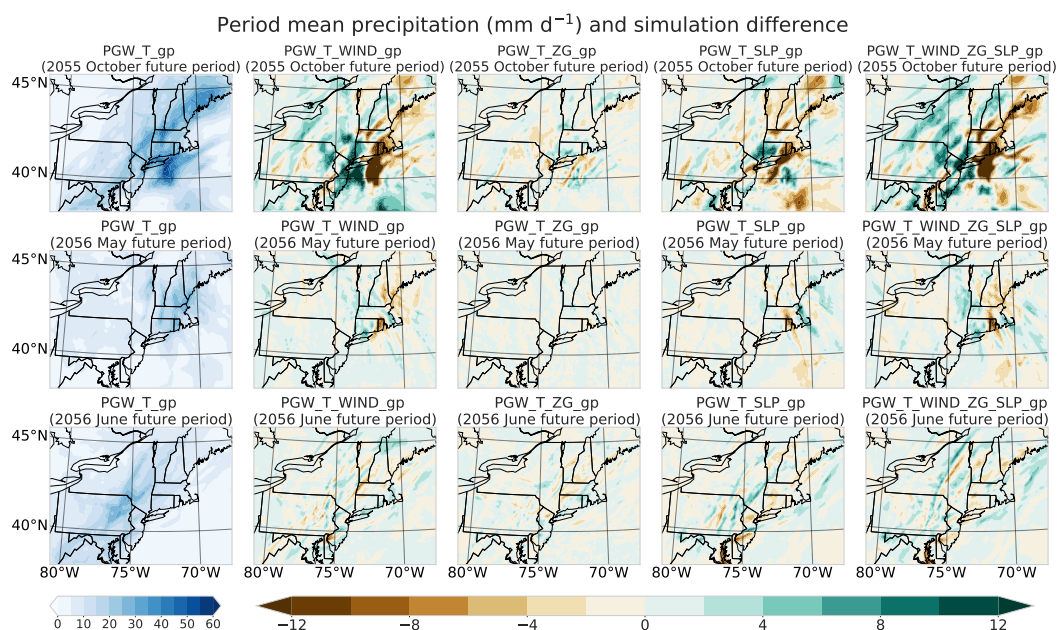
Figure 8. Period mean precipitation (mm d^{-1}) over the inner domain from the simulation with temperature perturbation at each gridpoint, and simulated differences in the simulations with dynamical perturbations of wind, geopotential height, sea level pressure and the combination of them at each gridpoint.
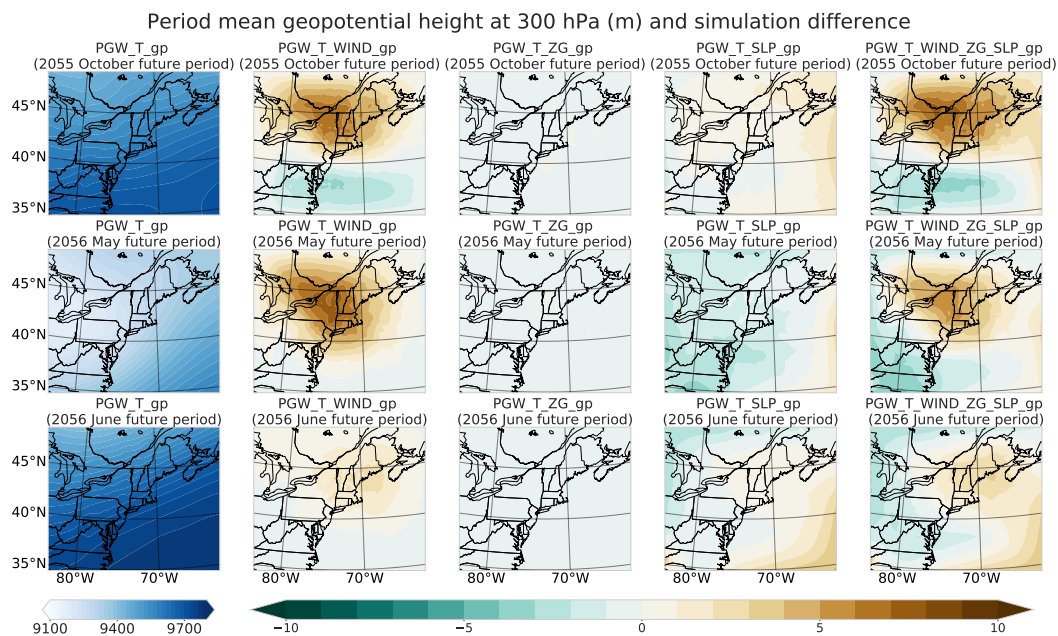
Figure 9. Period mean geopotential height and simulation deltas (m) at 300 hPa over the whole domain from the simulation with temperature perturbation at each gridpoint, and simulated perturbations in the simulations with additional dynamical perturbations of wind, geopotential height, sea level pressure and the combination of them at each gridpoint

3.4.2 Sensitivity of PGW simulations to inclusion of geopotential height perturbations

240   Among all the meteorological fields, modifying geopotential height (ZG) has the most insignificant impact on simulated precipitation: overall, the relative change in period regional mean precipitation is less than 1% (Fig. 6). This result is not unexpected, since the WRF Pre-Processing System (WPS) automatically applies vertical hydrostatic adjustments to produce a new geopotential height field that accords with the modified temperature fields via the hypsometric equation (Skamarock et al., 2008). Indeed, this is confirmed in Fig. 9, as we can see that even at 300 hPa, the simulation with geopotential height perturbations

245   applied produces a similar geopotential height output than our baseline simulation. Even when examining individual gridpoints, the simulation with modified ZG is largely indistinguishable from the baseline simulation (Fig. 8). Therefore, we do not recommend modification of the geopotential field in PGW studies, as it is unnecessarily redundant with the temperature perturbation.

3.4.3 Sensitivity of PGW simulations to inclusion of sea level pressure perturbations

250   From Fig. 8, the simulation with modified sea level pressure consistently produces less precipitation over both the land and sea area of the inner domain during all three flood periods. This reduction in precipitation arises from a largely positive sea level pressure perturbation over the whole sea area, which is the main source of moisture. From Fig. 10, in the simulations with

modified SLP, SLP perturbations are generally positive over the coastal and ocean areas and negative over the inland area. The magnitude of the positive SLP delta is larger during the first flood event (regional mean of 0.22 hPa) than the other two events

255   (regional means of 0.027 hPa and 0.16 hPa, respectively). Although the third flood event has a comparable regional-mean SLP perturbation to the first flood event over the sea, its SLP delta is negative over the inland regions of highest precipitation, while the other two flood events exhibit positive deltas. This results in the third flood event of the simulation with modified SLP having the smallest precipitation decrease over the inner domain (with the regional mean of -0.014 mm d^{-1} compared the other two events' -0.57 and -0.051 mm d^{-1}) (Fig. 8 and 6).

260   The most direct consequence of applying the SLP perturbation is a corresponding adjustment to regional near-surface temperature fields. This change emerges since WRF uses a hybrid vertical coordinate which is of roughly constant layer thickness at ground level, and so near-surface changes to SLP are incorporated at constant volume. By the hypsometric equation any increase (decrease) in SLP must be compensated for by a decrease (increase) in average layer temperature. Indeed, from Fig. 11, we can see that the simulation with modified SLP has significantly colder 2 meter temperatures in all three flood periods;

265   however, the third flood period is slightly different from the other two periods in that it does show some temperature enhancement throughout the NEUS. As the relative humidity is fixed among all simulations, colder temperature fields directly induce a reduction in precipitable water (Fig. 12). Overall, the regional period mean precipitable water decreases by 0.050, 0.083, and 0.027 mm in the three flood periods, respectively. Another consequence of a positive sea level pressure perturbation is suppressed convection during all three flood periods – and indeed we see the relative decrease of the regional period mean

270   convective available potential energy (CAPE) is 8.62%, 1.88%, and 5.34% over the ocean region (Fig. 13). In turn this reduces convective precipitation over the inner domain (with regional mean of -0.39, -0.19 and -0.04 mm d^{-1}, where again the third flood event has the smallest decrease). Moreover, the modified SLP field will impact wind fields (Fig. S6 and S7) and produce more obvious wave-like noises (Xue and Ullrich, 2022). Altogether, the simulation with modified SLP produces less precipitation overall.

275   It's clear that the inclusion of the SLP perturbation significantly weakens the warming signals from LE CESM (Fig. 7). For example, during the 2056 flood period, the regional mean temperature increase is 1.82 °C at 39th parallel north in PGW_T_gp; however, it drops to 1.00°C in the simulation with SLP perturbations (PGW_T_gp), which is less than a half of the warming signal (2.11°C) at the same latitude provided by LE CESM1 (Fig. 7). Consistent with our explanation above, the underestimation of the warming signal is constrained to the lowest model levels (Fig. 14). While those simulations not including the SLP

280   perturbation are largely consistent in the near-surface with the LE CESM1 average, inclusion of the SLP perturbation produces a strong divergence between WRF and the driving data. Because of this anomalous behavior, we recommend not including the SLP in PGW experiments.

4   Conclusions

Although there exist discrepancies among experiments with different PGW methods, the most significant gridpoint-level dif-

285   ferences emerge primarily from the displacement of storm events. If we look at the regional scale effects, relative differences
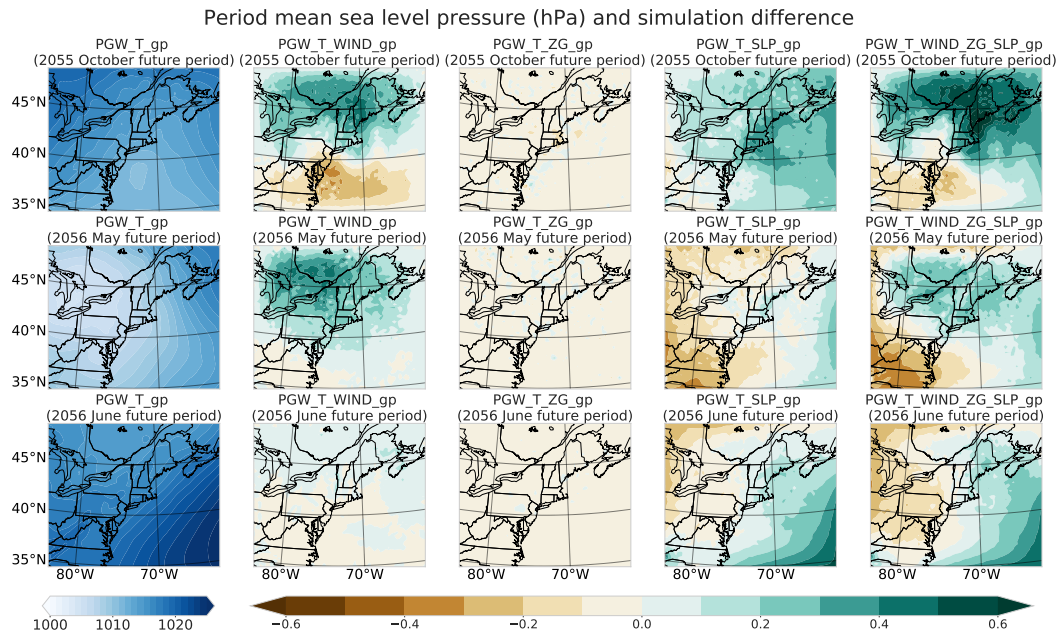
Figure 10. Period mean sea level pressure and simulation deltas (mm d^{-1}) over the whole domain from the simulation with temperature perturbation at each gridpoint, and simulated deltas when performing experiments with perturbations of wind, geopotential height, sea level pressure and their combination at each gridpoint.
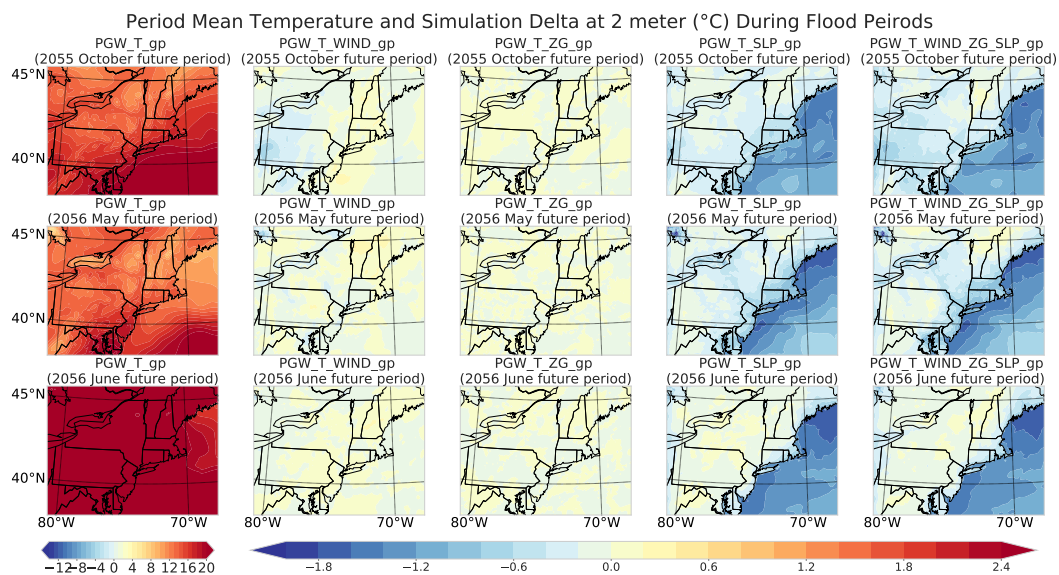
Figure 11. Period mean temperature and simulation deltas (°C) at 2 meter over the whole domain relative to the simulation with temperature perturbation at each gridpoint, and simulated deltas when performing experiments with perturbations of wind, geopotential height, sea level pressure and their combination at each gridpoint.
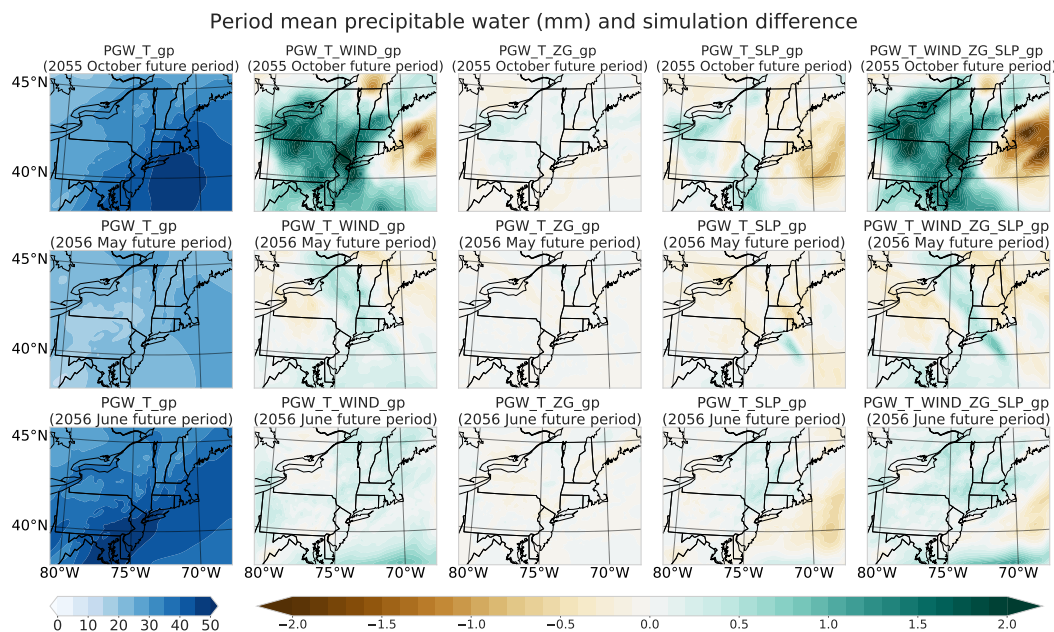
Figure 12. Period mean precipitable water and simulation deltas (mm) over the whole domain relative to the simulation with temperature perturbation at each gridpoint, and simulated deltas when performing experiments with perturbations of wind, geopotential height, sea level pressure and their combination at each gridpoint.

between different PGW experiments are less than 10%. We claim this study thus supports the robustness of the PGW method for projecting future change. With that said, there are some notable differences that suggest greater sensitivity of particular events to the experiment design: in particular, the 2005 October storm appears more sensitive to the choice of meteorological perturbations than the other two events. This is unsurprising, as certain storm events will be more "chaotic" than others – small

290 changes to the environment can result in significant changes in their subsequent behavior. Knowing that this event was driven by a passing cold front, while the other two were related to localized lows, may suggest greater sensitivity of frontal systems to the PGW experimental design. Of course, regardless of the underlying drivers of a particular event, at the regional mean scale the differences among PGW experiments tend to be relatively small.

Nonetheless, when choosing a particular PGW experiment design, one needs to be aware of the consequences of the partic-

295 ular design decisions being made. In this study, we found some common assumptions do not hold, and unrealistic results can emerge when choosing to perturb certain meteorological variables. In particular, we find that employing a regionally uniform temperature perturbation does not prevent the generation of spurious waves in the simulation; indeed, essentially all of our experiments did produce (climatologically insignificant) spurious waves during strong weather events. Additionally, we find that modifying the SLP in WRF leads to an underestimation the warming signal and produce stronger wave-like noises. These

300 limitations make PGW_T_regional and PGW_T_SLP_gp less favorable options for PGW experiments.

Within this study we are able to draw the following conclusions about sensitivity to experimental design:
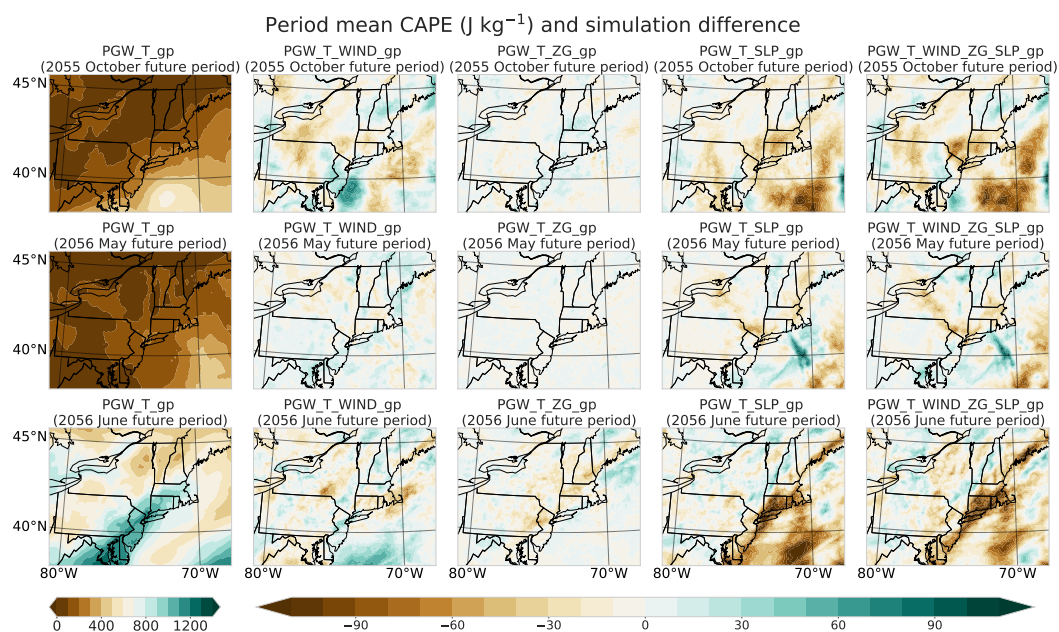
Figure 13. Period mean convective available potential energy (CAPE) and simulation deltas (J kg⁻¹) over the whole domain relative to the simulation with temperature perturbation at each gridpoint, and simulated deltas when performing experiments with perturbations of wind, geopotential height, sea level pressure and their combination at each gridpoint.
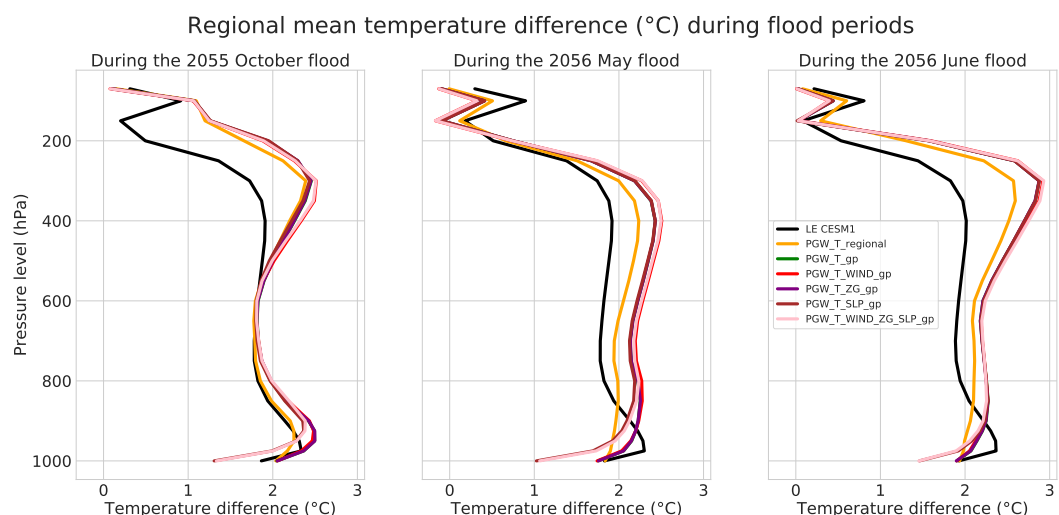
Figure 14. Period regional mean temperature differences (°C) at each pressure levels over the inner domain. The baseline is the historical flood period.

(1) The PGW experiment with regional mean temperature perturbation produced much higher precipitation totals than any experiment with gridpoint perturbations, since the experiment does not preserve discrepant changes in temperatures over the land and ocean.

305 (2) For experiments at the gridpoint scale, application of geopotential height perturbations does not appreciable modify the simulation in WRF. This is because this field will already be adjusted by the WRF Preprocessing System using the modified temperature fields.

(3) Gridpoint application of wind perturbations can appreciably impact the simulated precipitation because of the effect these perturbations have on vapor transport. Since the NEUS primarily receives precipitation from the southwest and on-
310 shore southwesterly winds are enhanced under future climate change, our experiments with wind perturbations generally show enhanced total overland precipitation during flood periods.

(4) Sea level pressure perturbations directly affect the temperature field, producing cooling where SLP is enhanced and warming where SLP is reduced. Since the SLP increase in our simulations is primarily over the ocean, these perturbations in turn reduce specific humidity and subseuqently reduce overland precipitation. SLP adjustments also affect CAPE and
315 lead to a reduction in convection and convective precipitation.

Based on the results of our analysis, we recommend perturbation of both temperature and wind at the gridpoint scale for future WRF-based PGW studies. This recommendation captures the spatially-dependent impacts of climate change on both thermodynamic and dynamic fields, without modifying unnecessary fields (i.e., geopotential height). Modifying both variables should (in theory) also reduce gravity wave noise, although we did not find an appreciable change in the presence of this noise
320 when wind perturbations were included. An alternative is to only include temperature perturbations at the gridpoint scale, which would enable isolation of the thermodynamical effects of climate change, and avoidance of the uncertain impact of climate change on dynamic fields.

As mentioned in the introduction, this study is not meant to be an exhaustive investigation of sensitivity of the PGW method to experiment design. Instead, our goal is to bring awareness to the impacts these choices can make in conclusions drawn from
325 PGW studies. We expect additional work is needed to investigate these sensitivies in other contexts (e.g., in inland areas or for other forms of extreme weather).

Data availability. The WRF model simulation data mentioned in this paper is available from ZENODO at 10.5281/zenodo.6609204.

Author contributions. Paul Ullrich and Zeyu Xue conceptualised this study and completed the manuscript. Zeyu conducted corresponding simulations on NERSC CORI.

330 *Competing interests.* The authors declare that they have no conflict of interest.

Acknowledgements. This research was supported by the RGMA and MSD program areas in the U.S. Department of Energy's Office of
Biological and Environmental Research as part of the multi-program, collaborative Integrated Coastal Modeling (ICoM) project with Contract
No. DE-AC05-76RL01830. This project is also supported by the National Institute of Food and Agriculture, U.S. Department of Agriculture,
hatch project under California Agricultural Experiment Station project accession no. 1016611. This research used resources of the National
335 Energy Research Scientific Computing Center (NERSC), a U.S. Department of Energy Office of Science User Facility located at Lawrence
Berkeley National Laboratory, operated under Contract No. DE-AC02-05CH11231 using NERSC award BER-ERCAP0020801. The authors
certify that they have no affiliations with or involvement in any organization or entity with any financial interest, or non-financial interest in
the subject matter or materials discussed in this manuscript.

References

340 Agel, L., Barlow, M., Qian, J.-H., Colby, F., Douglas, E., and Eichler, T.: Climatology of daily precipitation and extreme precipitation events
   in the northeast United States, Journal of Hydrometeorology, 16, 2537–2557, 2015.

   Beven, J.: Abbreviated Tropical Cyclone Report: Subtropical Depression Twenty-Two 8–10 October 2005, Tech. rep., National Hurricane
   Center, 2006.

   Blumen, W.: Geostrophic adjustment, Reviews of Geophysics, 10, 485–528, 1972.

345 Burns, D. A., Klaus, J., and McHale, M. R.: Recent climate trends and implications for water resources in the Catskill Mountain region, New
   York, USA, Journal of Hydrology, 336, 155–170, 2007.

   Center, N. C. D.: Climate of 2006 - June in Historical Perspective, https://web.archive.org/web/20070517170318/http://www.ncdc.noaa.gov/
   oa/climate/research/2006/jun/jun06.html, 2006a.

   Center, N. C. D.: Global Hazards And Significant Events, June 2006, https://web.archive.org/web/20070808002024/http://www.ncdc.noaa.
350 gov/oa/climate/research/2006/jun/hazards.html, 2006b.

   Center, N. C. D.: Climate of 2006 - May in Historical Perspective, https://web.archive.org/web/20070501091824/http://www.ncdc.noaa.gov/
   oa/climate/research/2006/may/may06.html, 2006c.

   Center, N. C. D.: Global Hazards And Significant Events, May 2006, https://web.archive.org/web/20070426090846/http://www.ncdc.noaa.
   gov/oa/climate/research/2006/may/hazards.html, 2006d.

355 Dai, A., Rasmussen, R. M., Ikeda, K., and Liu, C.: A new approach to construct representative future forcing data for dynamic downscaling,
   Climate Dynamics, 55, 315–323, 2020.

   Denamiel, C., Pranić, P., Quentin, F., Mihanović, H., and Vilibić, I.: Pseudo-global warming projections of extreme wave storms in complex
   coastal regions: the case of the Adriatic Sea, Climate Dynamics, 55, 2483–2509, 2020.

   Deser, C., Knutti, R., Solomon, S., and Phillips, A. S.: Communication of the role of natural variability in future North American climate,
360 Nature Climate Change, 2, 775–779, 2012.

   Deser, C., Phillips, A. S., Alexander, M. A., and Smoliak, B. V.: Projecting North American climate over the next 50 years: Uncertainty due
   to internal variability, Journal of Climate, 27, 2271–2296, 2014.

   Deser, C., Lehner, F., Rodgers, K., Ault, T., Delworth, T., DiNezio, P., Fiore, A., Frankignoul, C., Fyfe, J., Horton, D., et al.: Insights from
   Earth system model initial-condition large ensembles and future prospects, Nature Climate Change, pp. 1–10, 2020.

365 Dullaart, J. C., Muis, S., Bloemendaal, N., and Aerts, J. C.: Advancing global storm surge modelling using the new ERA5 climate reanalysis,
   Climate Dynamics, 54, 1007–1021, 2020.

   European Centre for Medium-Range Weather Forecasts: CESM Large Ensemble Data sets, NationalCenterforAtmosphericResearch, 2020a.

   European Centre for Medium-Range Weather Forecasts: ECMWF Reanalysis 5th Generation, https://www.ecmwf.int/en/forecasts/datasets/
   reanalysis-datasets/era5, 2020b.

370 Frei, C., Schär, C., Lüthi, D., and Davies, H. C.: Heavy precipitation processes in a warmer climate, Geophysical Research Letters, 25,
   1431–1434, 1998.

   Frumhoff, P. C., McCarthy, J. J., Melillo, J. M., Moser, S. C., and Wuebbles, D. J. e. a.: Confronting climate change in the US Northeast:
   Science, impacts, and solutions., Confronting climate change in the US Northeast: science, impacts, and solutions., 2007.

   Garner, S. T., Held, I. M., Knutson, T., and Sirutis, J.: The roles of wind shear and thermal stratification in past and projected changes of
375 Atlantic tropical cyclone activity, Journal of climate, 22, 4723–4734, 2009.

Hawkins, E. and Sutton, R.: The potential to narrow uncertainty in regional climate predictions, Bulletin of the American Meteorological Society, 90, 1095–1108, 2009.

Heikkilä, U., Sandvik, A., and Sorteberg, A.: Dynamical downscaling of ERA-40 in complex terrain using the WRF regional climate model, Climate dynamics, 37, 1551–1564, 2011.

380   Hersbach, H., Bell, B., Berrisford, P., Hirahara, S., Horányi, A., Muñoz-Sabater, J., Nicolas, J., Peubey, C., Radu, R., Schepers, D., et al.: The ERA5 global reanalysis, Quarterly Journal of the Royal Meteorological Society, 146, 1999–2049, 2020.

Hill, K. A. and Lackmann, G. M.: The impact of future climate change on TC intensity and structure: A downscaling approach, Journal of Climate, 24, 4644–4661, 2011.

Hirabayashi, Y., Mahendran, R., Koirala, S., Konoshima, L., Yamazaki, D., Watanabe, S., Kim, H., and Kanae, S.: Global flood risk under
385   climate change, Nature climate change, 3, 816–821, 2013.

Hobbs, J. J.: World regional geography, Nelson Education, 2008.

Huffman, G. J., Bolvin, D. T., Braithwaite, D., Hsu, K., Joyce, R., Xie, P., and Yoo, S.-H.: NASA global precipitation measurement (GPM) integrated multi-satellite retrievals for GPM (IMERG), Algorithm Theoretical Basis Document (ATBD) Version, 4, 26, 2015.

Jerez, S., López-Romero, J. M., Turco, M., Lorente-Plazas, R., Gómez-Navarro, J. J., Jiménez-Guerrero, P., and Montávez, J. P.: On the spin-
390   up period in WRF simulations over Europe: Trade-offs between length and seasonality, Journal of Advances in Modeling Earth Systems, 12, e2019MS001 945, 2020.

Karmalkar, A. V., Thibeault, J. M., Bryan, A. M., and Seth, A.: Identifying credible and diverse GCMs for regional climate change studies—case study: Northeastern United States, Climatic Change, 154, 367–386, 2019.

Kawase, H., Yoshikane, T., Hara, M., Kimura, F., Yasunari, T., Ailikun, B., Ueda, H., and Inoue, T.: Intermodel variability of future changes
395   in the Baiu rainband estimated by the pseudo global warming downscaling method, Journal of Geophysical Research: Atmospheres, 114, 2009.

Kay, J. E., Deser, C., Phillips, A., Mai, A., Hannay, C., Strand, G., Arblaster, J. M., Bates, S., Danabasoglu, G., Edwards, J., et al.: The Community Earth System Model (CESM) large ensemble project: A community resource for studying climate change in the presence of internal climate variability, Bulletin of the American Meteorological Society, 96, 1333–1349, 2015.

400   Kharin, V. V., Zwiers, F. W., Zhang, X., and Hegerl, G. C.: Changes in temperature and precipitation extremes in the IPCC ensemble of global coupled model simulations, Journal of Climate, 20, 1419–1444, 2007.

Kimura, F., Kitoh, A., Sumi, A., Asanuma, J., and Yatagai, A.: Downscaling of the global warming projections to Turkey, The Final Report of ICCAP, 10, 2007.

Knutson, T. R., Sirutis, J. J., Vecchi, G. A., Garner, S., Zhao, M., Kim, H.-S., Bender, M., Tuleya, R. E., Held, I. M., and Villarini, G.:
405   Dynamical downscaling projections of twenty-first-century Atlantic hurricane activity: CMIP3 and CMIP5 model-based scenarios, Journal of Climate, 26, 6591–6617, 2013.

Lackmann, G. M.: Hurricane Sandy before 1900 and after 2100, Bulletin of the American Meteorological Society, 96, 547–560, 2015.

Mallard, M. S., Lackmann, G. M., and Aiyyer, A.: Atlantic hurricanes and climate change. Part II: Role of thermodynamic changes in decreased hurricane frequency, Journal of climate, 26, 8513–8528, 2013a.

410   Mallard, M. S., Lackmann, G. M., Aiyyer, A., and Hill, K.: Atlantic hurricanes and climate change. Part I: Experimental design and isolation of thermodynamic effects, Journal of climate, 26, 4876–4893, 2013b.

Melillo, J. M., Richmond, T., and Yohe, G. e. a.: Climate change impacts in the United States, Third National Climate Assessment, 52, 2014.

Milly, P. C., Betancourt, J., Falkenmark, M., Hirsch, R. M., Kundzewicz, Z. W., Lettenmaier, D. P., and Stouffer, R. J.: Stationarity is dead: Whither water management?, Science, 319, 573–574, 2008.

415 Narayan, S., Beck, M. W., Wilson, P., Thomas, C. J., Guerrero, A., Shepard, C. C., Reguero, B. G., Franco, G., Ingram, J. C., and Trespalacios, D.: The value of coastal wetlands for flood damage reduction in the northeastern USA, Scientific Reports, 7, 1–12, 2017.

NOAA Physical Sciences Laboratory: CPC Unified Gauge-Based Analysis of Daily Precipitation over CONUS, https://psl.noaa.gov/data/gridded/data.unified.daily.conus.html, 2020.

Norris, J., Chen, G., and Neelin, J. D.: Thermodynamic versus dynamic controls on extreme precipitation in a warming climate from the
420 Community Earth System Model Large Ensemble, Journal of Climate, 32, 1025–1045, 2019.

Oravec, F.: Storm Summary Number 6, Tech. rep., The Hydrometeorological Prediction Center, 2006.

Pachauri, R. K., Allen, M. R., Barros, V. R., Broome, J., Cramer, W., Christ, R., Church, J. A., Clarke, L., Dahe, Q., Dasgupta, P., et al.: Climate change 2014: synthesis report. Contribution of Working Groups I, II and III to the fifth assessment report of the Intergovernmental Panel on Climate Change, Ipcc, 2014.

425 Pfahl, S., O'Gorman, P. A., and Fischer, E. M.: Understanding the regional pattern of projected future changes in extreme precipitation, Nature Climate Change, 7, 423–427, 2017.

Powers, J. G., Klemp, J. B., Skamarock, W. C., Davis, C. A., Dudhia, J., Gill, D. O., Coen, J. L., Gochis, D. J., Ahmadov, R., and Peckham, S. E. e. a.: The weather research and forecasting model: Overview, system efforts, and future directions, Bulletin of the American Meteorological Society, 98, 1717–1737, 2017.

430 Rasmussen, R., Liu, C., Ikeda, K., Gochis, D., Yates, D., Chen, F., Tewari, M., Barlage, M., Dudhia, J., Yu, W., et al.: High-resolution coupled climate runoff simulations of seasonal snowfall over Colorado: A process study of current and warmer climate, Journal of Climate, 24, 3015–3048, 2011.

Sato, T., Kimura, F., and Kitoh, A.: Projection of global warming onto regional precipitation over Mongolia using a regional climate model, Journal of Hydrology, 333, 144–154, 2007.

435 Schär, C., Frei, C., Lüthi, D., and Davies, H. C.: Surrogate climate-change scenarios for regional climate models, Geophysical Research Letters, 23, 669–672, 1996.

Sillmann, J., Kharin, V., Zhang, X., Zwiers, F., and Bronaugh, D.: Climate extremes indices in the CMIP5 multimodel ensemble: Part 1. Model evaluation in the present climate, Journal of Geophysical Research: Atmospheres, 118, 1716–1733, 2013.

Skamarock, W. C., Klemp, J. B., Dudhia, J., Gill, D. O., Barker, D. M., Wang, W., and Powers, J. G.: A description of the Advanced Research
440 WRF version 3. NCAR Technical note-475+ STR, Tech. rep., National Center for Atmospheric Research, 2008.

Station, M. W. O. W.: Preliminary Local Climatological Data over the Mount Washington Observatory Weather Station in October 2005, Tech. rep., Mount Washington Observatory Weather Station, 2005.

Stewart, S. R.: Tropical Cyclone Report: Tropical Storm Tammy 5-6 October 2005, Tech. rep., National Hurricane Center, 2006.

Stuart, N. and Grumm, R.: The use of ensemble and anomaly data to anticipate extreme flood events in the northeastern United States, NWA
445 Digest, 33, 185–202, 2009.

Swann, A. L., Hoffman, F. M., Koven, C. D., and Randerson, J. T.: Plant responses to increasing CO2 reduce estimates of climate impacts on drought severity, Proceedings of the National Academy of Sciences, 113, 10 019–10 024, 2016.

Tarek, M., Brissette, F. P., and Arsenault, R.: Evaluation of the ERA5 reanalysis as a potential reference dataset for hydrological modelling over North America, Hydrology and Earth System Sciences, 24, 2527–2544, 2020.

450 The National Aeronautics and Space Administration: Integrated Multi-satellitE Retrievals for GPM, https://gpm.nasa.gov/data/imerg, 2021.

Ullrich, P., Xu, Z., Rhoades, A., Dettinger, M., Mount, J., Jones, A., and Vahmani, P.: California's drought of the future: A midcentury recreation of the exceptional conditions of 2012–2017, Earth's Future, 6, 1568–1587, 2018.

US Bureau of Economic Analysis: Gross domestic product (GDP) by state (millions of current dollars) (2016 version), https://www.bea.gov/data/gdp/gdp-state, 2016.

455 Vecchi, G. A. and Soden, B. J.: Increased tropical Atlantic wind shear in model projections of global warming, Geophysical Research Letters, 34, 2007.

Wagener, T., Sivapalan, M., Troch, P. A., McGlynn, B. L., Harman, C. J., Gupta, H. V., Kumar, P., Rao, P. S. C., Basu, N. B., and Wilson, J. S.: The future of hydrology: An evolving science for a changing world, Water Resources Research, 46, 2010.

Wang, Y., Leung, L. R., McGREGOR, J. L., Lee, D.-K., Wang, W.-C., Ding, Y., and Kimura, F.: Regional climate modeling: progress,
460   challenges, and prospects, Journal of the Meteorological Society of Japan. Ser. II, 82, 1599–1628, 2004.

Xie, S.-P., Deser, C., Vecchi, G. A., Collins, M., Delworth, T. L., Hall, A., Hawkins, E., Johnson, N. C., Cassou, C., Giannini, A., et al.: Towards predictive understanding of regional climate change, Nature Climate Change, 5, 921–930, 2015.

Xu, Z. and Yang, Z.-L.: An improved dynamical downscaling method with GCM bias corrections and its validation with 30 years of climate simulations, Journal of Climate, 25, 6271–6286, 2012.

465 Xue, Z. and Ullrich, P.: A Comprehensive Intermediate-Term Drought Evaluation System and Evaluation of Climate Data Products over the Conterminous United States, Journal of Hydrometeorology, 22, 2311–2337, 2021a.

Xue, Z. and Ullrich, P.: A Retrospective and Prospective Examination of the 1960s U.S. Northeast Drought, Earth's Future, 9, xxx, 2021b.

Xue, Z. and Ullrich, P.: The sea level pressure animations during flood and dry periods, 10.5281/zenodo.6544880, 2022.

Yates, D., Luna, B. Q., Rasmussen, R., Bratcher, D., Garre, L., Chen, F., Tewari, M., and Friis-Hansen, P.: Stormy weather: Assessing climate
470   change hazards to electric power infrastructure: A Sandy case study, IEEE Power and Energy Magazine, 12, 66–75, 2014.